C-arm Tracking by Intensity-Based Registration of a Fiducial in Prostate Brachytherapy

Pascal Fallavollita[1], Clif Burdette[2], Danny Y. Song[3],
Purang Abolmaesumi[4], and Gabor Fichtinger[1]

[1] Queen's University, Canada
[2] Acoustic MedSystems Inc, Illinois
[3] Johns Hopkins Hospital, Baltimore
[4] University of British Columbia, Canada

Abstract. Motivation: In prostate brachytherapy, intra-operative dosimetry optimization can be achieved through reconstruction of the implanted seeds from multiple C-arm fluoroscopy images. This process requires tracking of the C-arm poses. Methodology: We compute the pose of the C-arm relative to a stationary radiographic fiducial of known geometry. The fiducial was precisely fabricated. We register the 2D fluoroscopy image of the fiducial to a projected digitally reconstructed radiograph of the fiducial. The novelty of this approach is using image intensity alone without prior segmentation of the fluoroscopy image. Experiments and Results: Ground truth pose was established for each C-arm image using a published and clinically tested segmentation-based method. Using 111 clinical C-arm images and ±10° and ±10 mm random perturbation around the ground-truth pose, the average rotation and translation errors were 0.62° (std=0.31°) and 0.73 mm (std= 0.55mm), respectively. Conclusion: Fully automated segmentation-free C-arm pose estimation was found to be clinically adequate on human patient data.

1 Introduction

Prostate cancer is the second most common cancer in men, diagnosed in 250,000 new patients each year in North America [1]. Brachytherapy is a definitive treatment of early stage prostate cancer, chosen by over 50,000 men each year with excellent long-term disease-free survival [2]. The procedure entails permanent implantation of small radioactive isotope capsules (a.k.a. seeds) into the prostate to kill the cancer with radiation. Success hinges on precise placement of the implants to provide the needed dose distribution. Unfortunately, primarily due to tissue motion, organ deformation, and needle deflection, implants never turn out to be as planned. Dynamic dosimetry optimization during the procedure would allow the physician to account for deviations from the plan and thus tailor the dose to cancer without harming surrounding healthy tissues. This requires localization of the prostate and the implanted seeds; a much coveted function that is not available today [3]. Prostate brachytherapy is performed with transrectal ultrasound guidance that provides adequate real-time visualization of the prostate but not of the implanted seeds. At the same time, C-arm fluoroscopy is

N. Navab and P. Jannin (Eds.): IPCAI 2010, LNCS 6135, pp. 45–55, 2010.

widely used for visual assessment and 3D reconstruction of the implanted seeds (Figure 1, left), but it cannot show the prostate and other relevant structures. Fusion of these two complementary modalities would enable dynamic dosimetry. A variety of fluoroscopic implant reconstruction and fusion techniques have been investigated [4-7]. These methods share one common requirement: the relative poses of the fluoroscopy images must be known prior to reconstruction.

Pose recovery on C-arm machines is a major technical problem that presently does not have a clinically practical solution in many areas of application. The relative poses of fluoroscopy images are determined in one of following three ways: (i) electronic joint encoders, (ii) optical or electromagnetic tracker, and (iii) radiographic fiducials. Fully encoded C-arms are very expensive and thus virtually non-existent in brachytherapy. External trackers are also impractical for various reasons and also add costs. Optical tracking[1,2] requires line of sight which imparts alterations in clinical setup and workflow. Electromagnetic tracking[3] overcomes these issues, but it is susceptible to field distortion from metal objects, such as the C-arm itself, and thus compromise on accuracy. Several researchers have explored fiducial-based radiographic tracking [8-11]. In an effort of making fiducials better integrated in the clinical setup, compact fiducials have been explored. Unfortunately, decreasing the size of the fiducial fixture also decreases tracking accuracy. In fiducial structures made up of beads, the typical number of beads was between 6 and 28. With these structures, researchers achieved 1-3 mm translation accuracy and 1°–2° orientation accuracy in tracking the C-arm [9-11]. Accuracy was primarily governed by bead configuration [9] and implementation [10] choices. In all, the best accuracy that bead-shape fiducials can achieve is about 1 mm error in translation and 1° error in rotation.

For prostate brachytherapy Jain *et al.* developed a fluoroscope tracking (FTRAC) fiducial [12] and validated the device clinically [7]. In addition to spherical beads, they used straight lines and ellipses that are invariant to projection, in that they project as straight lines and ellipses (Figure 1, center). Such parametric curves segment accurately and constrain the optimization during pose recovery, allowing for a mean accuracy of 0.56 ± 0.33mm in translations and 0.33°± 0.21° in rotations [12]. The FTRAC design has small dimensions (3x3x5cm), no special proximity requirements to the anatomy, and is relatively inexpensive. They mounted the FTRAC fiducial over the seed insertion needle template using a mechanical connector (Figure 1, right) [7]. After semi-automatic segmentation of the FTRAC fiducial in all C-arm images, the implanted seeds were reconstructed in 3D, registered with transrectal ultrasound space and sent back to the treatment planning system for dosimetric evaluation. In this process, the single point of failure is segmentation of the FTRAC. Sequential semi-automated segmentation of different features of the FTRAC was found to be fragile in actual field practice [7].

In essence, Jain *et al.* computed a registration between the 3D geometrical model of their tracking fiducial and its 2D projection pre-segmented in the C-arm image: i.e. they performed a 2D/3D registration. Prior work in 2D/3D registration algorithms can be divided into two major categories: feature-based and intensity-based methods. The

[1] VectorVision® Navigation System, "Brainlab, Inc., Heimstetten, Germany.
[2] StealtStation®, Medtronic Surgical Navigation Technologies, Louisville, CO, USA.
[3] OEC 9800 FluoroTrak™, GE Healthcare, Waukesha, WI, USA.

former, such as [15-17], use distance between corresponding point pairs or surfaces as a measure to be optimized. Establishing point correspondences and minimizing the distance between them is alternated and repeated iteratively until convergence. Consequently, prior segmentation of the image data is required. Many researchers in computer vision have tried to recover pose based on point features. For calibrated cameras the so called five-point algorithm has been used extensively [18]. This method can cope with planar scenes, but in case of more than five points it computes multiple solutions. Minimal solvers are of importance for algorithms like random consensus sampling [19] to establish unknown correspondences between the features across images. Intensity-based methods compare the 2D image with a digitally reconstructed radiograph (DRR) created from the 3D volume. One can compare the imprints of anatomical structures obtained from either gradient information or voxel intensity [20-22].

We propose computing the relative pose of C-arm images by the registration of fluoroscopy image to a radiographic fiducial, without segmentation, with an accuracy that is sufficient for subsequent reconstruction of brachytherapy seeds. While all computational components used have been previously described by others, this should not belie the investment of creative effort required for devising a clinically practical approach and testable embodiment. We present methodology, implementation, and performance analysis on clinical patient data.

Fig. 1. *Left*: Prostate brachytherapy setup using transrectal ultrasound imaging to visualize the prostate and C-arm fluoroscopy to assess seed positions. *Center*: Sketch of the FTRAC fluoroscope tracking fiducial. *Right:* The fiducial is mounted and affixed to the needle insertion template during the procedure.

2 Methodology

2.1 Hypothesis

Our hypothesis is that the C-arm pose can be recovered adequately using a 2D/3D intensity-based registration algorithm between the fiducial's C-arm image and the

fiducial's known geometrical model. For proving the concept, we used the aforementioned FTRAC fiducial introduced by Jain *et al*. [12] (Figure 1, right). The proposed 2D/3D registration scheme, depicted in Figure 2, follows several steps. (1) Calibrate the C-arm explicitly or assume a sufficiently accurate model of it. (2) Filter the fluoroscopy image to simultaneously enhance FTRAC features and to suppress neighboring structures. (3) Take an initial guess for pose of the C-arm relative to FTRAC. (4) Compute a DRR of the FTRAC. (5) Apply blurring operator on the lines/features in the DRR. (6) Run 2D/3D optimization to compute the pose using a normalized cross correlation metric and an Evolution Strategy with Covariance Matrix Adaptation (CMA-ES) optimizer. Adjust the C-arm pose and step back to (4) until convergence is achieved or failure to converge is detected.

2.2 C-arm Image Filtering

C-arm images are characterized by a low signal-to-noise ratio inducing image artifacts such as motion blur (i.e. object are blurred or smeared along the direction of relative motion). A three-step filter is used to diminish the negative effects of artifacts. All filter parameter definitions are listed in Table 1 and explained below.

2.2.1 Morphological Filtering

Morphological filtering is applied in grayscale to suppress the background of the C-arm image and enhance the FTRAC features. The structuring element chosen was in the shape of a disk of small radius, since the ball bearing and ellipse perimeter making up the FTRAC can be modeled as disk elements of small size. The morphological operator has only one filter parameter, which is the size of the structuring element.

2.2.2 Homomorphic Filtering

A homomorphic filter is used to de-noise the C-arm image. It sharpens features and flattens lighting variations in the image. The illumination component of an image is generally characterized by slow spatial variation while the reflectance component of an image tends to vary abruptly. These characteristics lead to associating the low frequencies of the Fourier transform of the natural log of an image with illumination and high frequencies with reflectance. Kovesi [23] provides excellent insights to the use of homomorphic filter. Even though these assumptions are approximation at best, a good deal of control can be gained over the illumination and reflectance components with a homomorphic filter. For the homomorphic filter to be effective, it needs to affect the low- and high-frequency components of the Fourier transform differently. To compress the dynamic range of an image, the low frequency components need to be attenuated to some degree. At the same time, in order to enhance the contrast, the high frequency components of the Fourier transform needs to be magnified. Thus Butterworth low and high pass filters are implemented and the image histograms are truncated accordingly.

2.2.3 Complex Shock Filtering

Gilboa *et al*. [24] have developed a filter coupling shock and linear diffusion in the discrete domain. The shock filter's main properties are the following: (i) shocks develop at inflection points (i.e. second derivative zero-crossings), (ii) local extrema

remain unchanged in time, (iii) the scheme is total variation preserving, (iv) the steady state (weak) solution is piece-wise constant, and finally (v) the process approximates deconvolution. Unfortunately, noise in the blurred signal will also be enhanced. Robustness to noise can be improved by convolving the signal's second derivative with a Laplacian of Gaussian filter. This, however, is generally not sufficient to overcome the noise problem entirely, because convolving the signal with a Gaussian of moderate width in many cases will not cancel the inflection points produced by noise [24]. In order to alleviate this problem, a more complex approach is suggested: smoother parts are denoised while edges are enhanced and sharpened. The complex shock filter is hereby given by:

$$I_{t=-}\frac{2}{\pi}\arctan\left(aIm\left(\frac{I}{\theta}\right)\right)|\nabla I| + \lambda I_{\eta\eta} + \tilde{\lambda} I_{\xi\xi} \tag{1}$$

where a is a parameter that controls the sharpness of the slope, $\lambda = re^{i\theta}$ is a complex scalar, $\tilde{\lambda}$ is a real scalar, ξ is the direction perpendicular to the gradient and η is the direction of the gradient. In this way the inflection points are not of equal weight anymore; regions near edges with a large magnitude of second derivative near the zero crossing will be sharpened much faster than relatively smooth regions [24].

Table 1. Three step filter parameter definitions and assigned values, (parameter units in parenthesis)

	Filter Definitions	Value
I.	**Morphology filter**	
	- Structuring element size (radius in pixels)	2
II.	**Homomorphic filter**	
	- boost ratio of high frequency relative to low frequency	2
	- cutoff frequency of the filter	0.05
	- order for low and high pass Butterworth filters	3
	- truncation of the lower end of the image histogram	5
	- truncation of the higher end of the image histogram	0.01
III.	**Complex Shock Filter**	
	- number of iteration	10
	- time step size	1
	- grid step size	0.1
	- magnitude of the complex diffusion in the gradient direction	0.1
	- amount of diffusion in the level set direction	0.5
	- slope of the arctangent	0.3
	- phase angle of the complex term (in radians)	π/1000

2.3 Single-View Registration

We apply 2D/3D registration considering the DRR as the moving image and the C-arm image as the fixed image. We used MATLAB R2008a for implementation purposes.

As we only use one C-arm image at a time, to estimate the pose for that image, we termed this single-view registration, explained by the flowchart in Figure 2.

Metric: We implemented the normalized cross correlation metric that considers all pixel values in the images during registration. Fixed image pixels and their positions are mapped to the moving image. The correlation is normalized by the autocorrelations of both the fixed and moving images. The normalized cross correlation metric minimizes a cost function and the registration parameters will be optimal when minimum cost is reached.

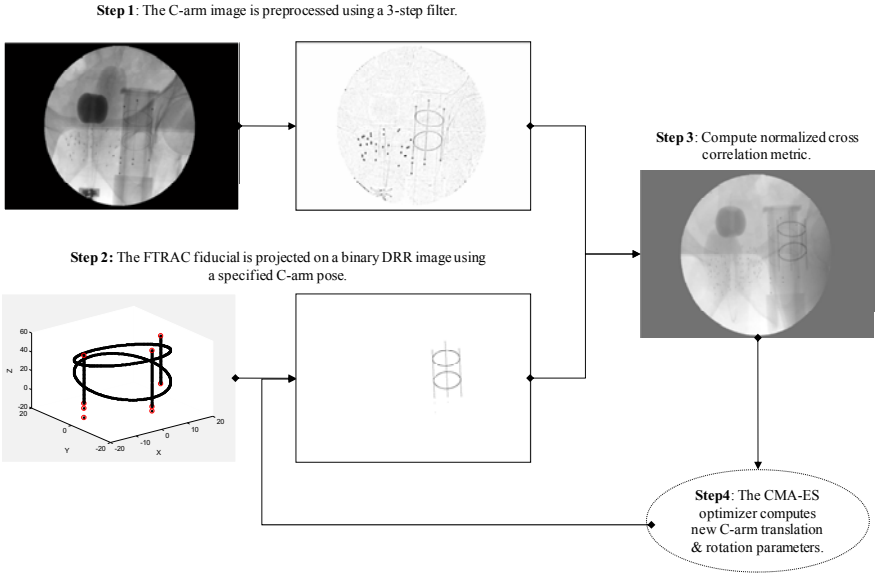

Fig. 2. C-arm pose recovery algorithm flowchart. (1) C-arm image is filtered by the 3-step filter to enhance FTRAC features while suppressing background structures. (2) FTRAC projected as a binary DRR image at a specified C-arm pose. (3) A normalized cross correlation metric computed. (4) CMA-ES optimizer computes new pose, process steps back to (2), until convergence or failure to convergence.

Transform: As the FTRAC is a rigid mechanical structure, rigid registration suffices. We implemented a transformation of six parameters, with three for Euler angles and three for translation.

Initial Guess: In the operating room, we have a consistently good initial guess for the registration. Standard patient positioning allows for aligning the main axes of the FTRAC, transrectal ultrasound and C-arm, enabling us to compute a gross registration in the anterior-posterior pose of the C-arm. Additional C-arm images are acquired according to a set protocol at 15° increments.

DRR Generation: The FTRAC fiducial is projected on a two dimensional binary image and blurred using a Gaussian filter. The filter parameters that need to be

considered during implementation are the kernel size, kernel, and the sigma (σ) used for the Gaussian kernel.

Optimizer: The CMA-ES is an evolutionary algorithm for difficult non-linear non-convex optimization problems in continuous domain. In contrast to quasi-Newton methods, the CMA-ES does not use or approximate gradients and does not even presume or require their existence. This makes the method applicable to non-smooth and even non-continuous problems, as well as to multimodal and/or noisy problems [25]. The CMA-ES has several invariance properties. Two of them, inherited from the plain evolution strategy, are (i) invariance to order preserving (i.e. strictly monotonic) transformations of the objective function value and (ii) invariance to angle preserving (rigid) transformations of the search space (including rotation, reflection, and translation), if the initial search point is transformed accordingly. The CMA-ES does not require a tedious parameter tuning for its application. With the exception of population size, tuning of the internal parameters is not left to the user [25].

3 Results and Discussion

3.1 Registration Evaluation

We recall the primary objective of this work: provide an estimation of the C-arm fluoroscope poses for subsequent brachytherapy implant reconstruction. The implant reconstruction of Jain *et al.* requires curtailing the pose estimation error to ±4° in rotation and to ±2 mm in lateral translation [13]. In 2D/3D registration, the cost metric usually has difficulties with properly "driving" the depth component of the pose. In C-arm reconstruction, however, the exact same effect is working for our advantage, because the reconstruction metric is similarly insensitive to the depth component of the C-arm pose. Jain *et al.* found that "reconstruction error is insensitive to miscalibration in origin and focal length errors of up to 50 mm", inferring that even large depth errors are permissible if all image poses shift together [14]. What follows is that if the prostate is kept near the isocenter, projection and reconstruction are both insensitive to depth.

The registration error was evaluated against the C-arm pose obtained from ground truth (i.e. average errors of 0.56mm and 0.33º obtained by the FTRAC fiducial). In this paper, the values for mean registration error and standard deviations were calculated as the difference obtained from the ground truth and the registration, respectively. Capture range was defined as the range within which the algorithm is more likely to converge to the correct optimum. We applied random misalignment of maximum ±10 mm translation and ±10 degree rotation to ground truth obtained by segmenting the FTRAC and recovering pose. This capture range, especially for rotation, is larger than the error of the initial guess one can achieve clinically. We set the number of iterations for the optimizer to 30 and the population size at 65, resulting in 98.5% algorithm convergence. Using a total of 13 patient datasets, we performed the registration 25 times for each of the 111 clinical C-arm patient images, acquired under ethics board approval.

3.2 Results

The filter parameters were determined empirically by using a subsample of 10 C-arm images, with varying initial contrast, and fine-tuning the values so that the FTRAC features are always enhanced with respect to their neighborhood. Values for the proposed 3-Step filter are listed in Table 1. For the DRR binary image Gaussian smoothing, the sigma value was set to σ=1.5 pixels.

The performance of our proposed filter is presented in Figure 3. First, we observe that image contrast differs between patients. However, the chosen filter parameters improved the robustness and performance of our proposed filter; the pelvic bone and other neighboring structures were suppressed successfully while both the FTRAC fiducial and implanted seeds were enhanced. The filtered C-arm image was given as input to our intensity-based registration algorithm.

Five of the six degrees of freedom parameters were consistently below 0.5 mm and 1°. Using 111 clinical C-arm images and ±10° and ±10 mm random perturbation, the average rotation and translation errors were 0.62° (std=0.31°) and 0.73 mm (std= 0.55mm), respectively. As expected, the single view registration process did not recover the depth robustly (T_z parameter), yet on average the value is below clinical requirement of 2 mm.

Table 2. Final single-view registration results for 111 C-arm images

±10 mm and ±10° perturbation			
Tx (mm)	Ty (mm)	Tz (mm)	Rotations (degree)
0.14±0.08	0.11±0.16	1.9±1.4	0.6±0.3

3.3 Discussion

Of the 2775 trials, only 36 showed failure in registration convergence. Approximately half of the failures were due to the FTRAC fiducial being positioned near the black circular mask of the C-arm images (Figure 3, right), meaning that some features such as the top ball bearings and part of the top ellipse were not visible in the image. Also, since we started the registration from random initial guess, some runs were launched from an initial guess that projected the FTRAC outside the fluoroscopy image into the black mask where there was no feature guide the optimization into the image. We did not rerun registration with new initial guess since the purpose of the study was to show the true viability and robustness of our registration algorithm in a single run. Nevertheless, we expect the reported results in Table 2 to improve with restarting the registration process and/or with launching from an initial guess that projects the FTRAC within the C-arm image.

For the un-optimized MATLAB prototype implementation, a typical registration took about 170 seconds per image with Intel Core2, 2.4 GHz, dual-core computer. Figure 4 shows images after registration of binary FTRAC and C-arm images. A useful byproduct of our registration scheme is implicit and automatic segmentation of the radiographic fiducial, allowing the clinical user to visually approve the result of registration.

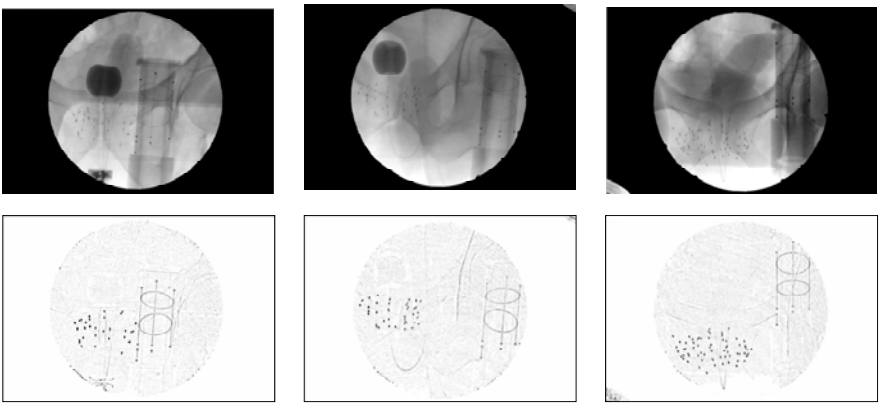

Fig. 3. C-arm image filtering. Here, three sample clinical images from three different patients with varying contrast. The morphology, homomorphic and shock filters smooth the image and enhance both the implanted seeds and FTRAC features while suppressing neighboring structures.

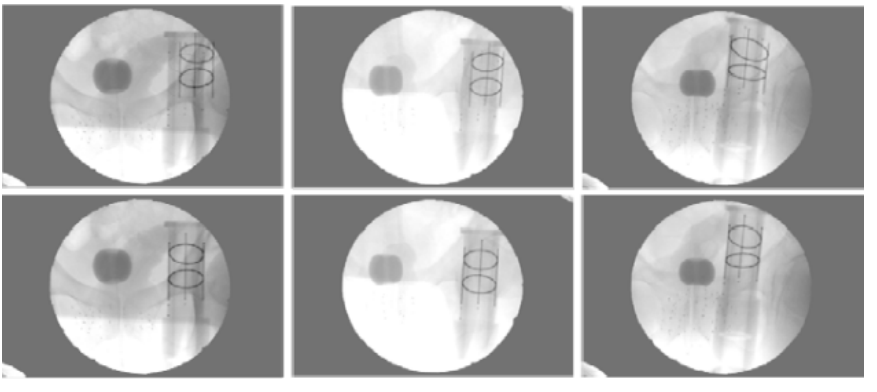

Fig. 4. Sample results before and after registration. With respect to original FTRAC size, initial perturbations had the same scale (*left*), smaller scale (*center*), and larger scale (*right*). The final overlay shows accurate superposition of the FTRAC fiducials. We note the 1 cm error in translations as initial perturbation for the left image.

Follow-up work will focus on adaptive filtering to compensate for varying C-arm image quality. Ideally, adaptive filter will analyze the image histograms and select optimal filter parameters accordingly. As of now, the parameters were empirically chosen and were found to be adequately robust in processing all available images. In order to test this approach prospectively in clinical trial, running time must be reduced below 1 minute per pose. As C-arm images are acquired by a well-defined protocol, we always know in which area of the C-arm the fiducial will appear, which in turn enables us to crop the C-arm image and thus reduce computation time. Additional speedup will be obtained from recoding the registration in C++.

4 Conclusion

In summary, we presented the first report of C-arm pose recovery by intensity-based registration of projected images of a geometrical model of a fluoroscope tracking fiducial and its C-arm images. Fluoroscopy images were pre-treated with a three-step filter that was found to be robust to varying image quality experienced in 111 C-arm images from 13 patients. Retrospective analysis of patient data showed clinically sufficient accuracy.

References

[1] Jemal, A., Siegel, R., Ward, E., et al.: Cancer Statistics. CA Cancer J. Clin. 59(4), 225–249 (2009)

[2] Zelefsky, M.J., Kuban, D.A., Levy, L.B., et al.: Multi-institutional analysis of long-term outcome for stages T1-T2 prostate cancer treated with permanent seed implantation. Int. J. Radiat. Oncol. Biol. Phys. 67(2), 327–333 (2007)

[3] Nag, S., Ciezki, J.P., Cormack, R., et al.: Intraoperative planning and evaluation of permanent prostate brachytherapy: report of the American Brachytherapy Society. Int. J. Radiat. Oncol. Biol. Phys. 51(5), 1422–1430 (2001)

[4] Orio, P.F., Tutar, I.B., Narayanan, S., et al.: Intraoperative ultrasound-fluoroscopy fusion can enhance prostate brachytherapy quality. Int. J. Radiat. Oncol. Biol. Phys. 69(1), 302–327 (2007)

[5] Westendorp, H., Hoekstra, C.J., van't Riet, A., et al.: Intraoperative adaptive brachytherapy of iodine-125 prostate implants guided by C-arm cone-beam computed tomography-based dosimetry. Brachytherapy 6(4), 231–237 (2007)

[6] Su, Y., Davis, B.J., Furutani, K.M., et al.: Seed localization and TRUS- fluoroscopy fusion for intraoperative prostate brachytherapy dosimetry. Computer Aided Surgery 12(1), 25–34 (2007)

[7] Jain, A.K., Deguet, A., Iordachita, I., et al.: Intra-operative Guidance in Prostate Brachytherapy Using an Average Carm. In: Ayache, N., Ourselin, S., Maeder, A. (eds.) MICCAI 2007, Part II. LNCS, vol. 4792, pp. 9–16. Springer, Heidelberg (2007)

[8] Yao, J., Taylor, R.H., Goldberg, R.P., et al.: A C-arm fluoroscopy-guided progressive cut refinement strategy using a surgical robot. Comput. Aided Surg. 5, 373–390 (2000)

[9] Zhang, M., Zaider, M., Worman, M., Cohen, G.: On the question of 3d seed reconstruction in prostate brachytherapy: the determination of x-ray source and film locations. Phys. Med. Biol. 49, 335–345 (2004)

[10] Yaniv, Z., Joskowicz, L.: Precise robot-assisted guide positioning for distal locking of intramedullary nails. IEEE Trans. Med. Imaging 24, 624–635 (2005)

[11] Tang, T.S.Y., MacIntyre, N.J., Gill, H.S., et al.: Accurate assessment of patellar tracking using fiducial and intensity-based fluoroscopic techniques. Med. Image Anal. 8, 343–351 (2004)

[12] Jain, A.K., Mustufa, T., Zhou, Y., et al.: FTRAC–a robust fluoroscope tracking fiducial. Medical physics 32(10), 3185–3198 (2005)

[13] Jain, A., Fichtinger, G.: C-arm Tracking and Reconstruction without an External Tracker. In: Larsen, R., Nielsen, M., Sporring, J. (eds.) MICCAI 2006, Part I. LNCS, vol. 4190, pp. 494–502. Springer, Heidelberg (2006)

[14] Jain, A., Kon, R., Zhou, Y., et al.: C-arm calibration - is it really necessary? In: Duncan, J.S., Gerig, G. (eds.) MICCAI 2005. LNCS, vol. 3749, pp. 639–646. Springer, Heidelberg (2005)
[15] Gueziec, A., Wu, K., Kalvin, A., et al.: Providing visual information to validate 2-d to 3-d registration. Medical Image Analysis 4, 357–374 (2000)
[16] Zuffi, S., Leardini, A., Catani, F., et al.: A model-based method for the reconstruction of total knee replacement kinematics. IEEE Trans. Med. Imag. 18(10), 981–991 (1999)
[17] Yamazaki, T., Watanabe, T., Nakajima, Y., et al.: Improvement of depth position in 2d/3d registration of knee implants using single-plane fluoroscopy. IEEE Trans. on Medical Imaging 23(5), 602–612 (2004)
[18] Nister, D.: An efficient solution to the five-point relative pose problem. IEEE Trans. on Pattern Analysis and Machine Intelligence 26(6), 756–770 (2004)
[19] Fischler, M., Bolles, R.: Random sample consensus: A paradigm for model fitting with applications to image analysis and automated cartography. Comm. Assoc. Comp. Mach. 24(6), 381–395 (1981)
[20] Livyatan, H., Yaniv, Z., Joskowicz, L.: Gradient-based 2-D/3-D rigid registration of fluoroscopic X-ray to CT. IEEE Trans. Med. Imaging 22, 1395–1406 (2003)
[21] Mahfouz, M., Hoff, W., Komistek, R., Dennis, D.: A robust method for registration of three-dimensional knee implant models to two-dimensional fluoroscopy images. IEEE Transactions on Medical Imaging 22, 1561–1574 (2003)
[22] Lau, K., Chung, A.: A global optimization strategy for 3d-2d registration of vascular images. In: Proceedings of 17th British Machine Vision Conference, pp. 489–498 (2006)
[23] Kovesi, P.: Functions for Computer Vision and Image Processing (2009), http://www.csse.uwa.edu.au/~pk/research/matlabfns/
[24] Gilboa, G., Sochen, N., Zeevi, Y.: Regularized shock filters and complex diffusion. In: Heyden, A., Sparr, G., Nielsen, M., Johansen, P. (eds.) ECCV 2002. LNCS, vol. 2350, pp. 399–413. Springer, Heidelberg (2002)
[25] Hansen, N.: The CMA Evolution Strategy: A Comparing Review. Studies in fuzziness and soft computing 192, 75–102 (2006)